To Luminesce or to Change Valence? Insight into the Wavelength Dependency of the Reversible Valence Switching of Europium in Sr_3SiO_5

Jieqi Hu[1,2], Zetian Yang[1], Ang Feng[1], Rik Van Deun[2], Philippe F. Smet[1], David Van der Heggen[1,]*

[1] LumiLab, Department of Solid State Sciences, Ghent University, Krijgslaan 281-S1, 9000 Gent.

[2] L^3 – Luminescent Lanthanide Lab, Department of Chemistry, Ghent University, Krijgslaan 281-S3, 9000 Gent.

KEYWORDS: strontium silicate; charge transfer; luminescence; spectroscopy; optical information storage.

ABSTRACT: A good control over the valence state of dopants in luminescent materials or phosphors is important for the development highly efficient phosphors for white LEDs. Detailed spectroscopic studies allow to reveal optically induced charge transfer processes and elucidate the underlying mechanisms in phosphors with additional functionalities such as photochromism or persistent luminescence. However, the spectroscopic study of the valence switching of europium has scarcely been reported. Here we report on the Sr_3SiO_5:Eu phosphor, in which

photo-reduction ($Eu^{3+} \rightarrow Eu^{2+}$) and photo- or thermal-oxidation ($Eu^{2+} \rightarrow Eu^{3+}$) reactions are demonstrated. Variation of the illumination wavelength influences both the efficiency of the photo-reduction/oxidation and the accompanying dynamic process, especially when the two opposite reactions simultaneously occur. Temperature-dependent annealing indicates a large trap depth for the electron trapped by Eu^{3+}. The good stability of Eu^{2+} obtained by photo-reduction and the repeatability of the Eu^{2+}/Eu^{3+} valence switching are confirmed as well. Furthermore, the application of optical information storage is demonstrated based on this phosphor. The results in this work may not only improve the understanding of Eu^{2+}/Eu^{3+} valence change during illumination, but also allow the development of new functional luminescent materials.

1. INTRODUCTION

The introduction of lanthanide activators in inorganic host materials laid the foundation for many modern optical applications such as lasers, telecommunication, solid-state lighting and displays.[1,2] Most of these widely-used luminescent lanthanide elements are most stable in the trivalent oxidation state, but some of them can also be incorporated in a divalent or tetravalent state with different optical behavior.[3-5] This multivalent nature of lanthanide ions enables charge transfer processes between two non-equivalent lanthanide ions or a lanthanide ion and a trapping defect, leading to versatile functional behaviors. For example, metastable charge transfer states involving a lanthanide and another defect can give rise to persistent luminescence, optically stimulated luminescence (OSL), spectral hole-burning and photochromism.[6-11] In addition, the unstable charge transfer state may result in energy transfer, so-called anomalous emission, or exotic metal-to-metal charge transfer (MMCT) luminescence, which merits special consideration for developing new phosphors.[12-14]

In some cases, however, it is found that charge transfer processes bring about unfavorable luminescence quenching, which has been proven to occur not only in co-doped systems such as those containing Ce^{3+}-Eu^{3+} or Pr^{3+}-Eu^{3+}, but also in Eu^{2+}-doped phosphors with even a small fraction of Eu^{3+}.[15-17] The presence of both Eu^{2+} and Eu^{3+} is almost inevitably present in most Eu^{2+}-doped phosphors even if they are prepared under reducing conditions.[17] Electron transfer can occur between Eu^{2+} and Eu^{3+}, and this process is then classified as intervalence charge transfer (IVCT) in which two metal sites differ only in oxidation state. The corresponding IVCT state provides a new nonradiative decay channel towards the relaxed mixed-valence ground state, thus leading to the Eu^{2+} emission being partially or even totally quenched.[17,18] Even though undesired Eu^{3+} may show weak or even non-detectable emission, this fraction can still have a considerable quenching effect on the Eu^{2+} emission, possibly through such an IVCT process, thereby lowering the quantum efficiency of the phosphor.[19-22] It should also be mentioned that besides incomplete reduction of Eu^{3+} during synthesis, Eu^{3+} can also be formed by prolonged or strong excitation as encountered in the case of high-power white LEDs or laser-driven solid-state lighting, which is still a big issue for these applications.[21,23] Sometimes, however, the opposite process is undesired and suppression of the formation of divalent lanthanides is needed. For example, a process referred to as photodarkening occurs in Yb^{3+}-doped optical fibers with simultaneous generation of undesired Yb^{2+} ions and hole centers under illumination, which induces optical losses and consequently degrades the fiber's performance for high-power laser in long-term operations.[24,25] All these phenomena highlight the importance of being able to deliberately control and stabilize the valence state of lanthanide activators for targeted optical applications.

When considering the divalent lanthanide ions, Eu^{2+}, Yb^{2+}, Sm^{2+} are the most common ones due to their relatively low Ln^{3+}/Ln^{2+} reduction potentials.[4] The oxidation state of these lanthanide activators can thus be tuned between the divalent and the trivalent state. Usually, for Ln^{3+} activators, sufficiently oxidizing conditions are achieved by performing the synthesis in air.[26] While for Ln^{2+} activators, they can typically be obtained by employing reducing conditions offered by reducing atmosphere (e.g., H_2, CO) or agents (e.g., CaH_2, NaH, LiH).[19,27] Intrinsic reduction of Ln^{3+}, i.e., preferential stabilization of Ln^{2+} without reducing conditions, has also been reported in some hosts. SrB_4O_7 is the most prominent representative owing to the appropriate rigid crystal structure and underlying charge-compensating defects.[28,29] Chemical substitution, electron beam annealing, and electrochemical reduction can also be utilized to regulate the valence state of lanthanide ions.[30-33] Besides, post-treatment with photo-irradiation can result in stable Ln^{2+} following photo-reduction from Ln^{3+} to Ln^{2+}. For higher photon energies or densities, irradiation with X-ray, γ-ray or femtosecond laser pulses at a nonresonant energy level create free electrons which can then be captured by Ln^{3+} to form Ln^{2+}.[34,35] UV or resonant stepwise multiphoton absorption may also induce photo-reduction processes, presumably with the participation of a photochemically active charge transfer state.[25,36-38] The Ln^{2+} obtained by photo-reduction can be oxidized again by thermal stimulation, photo-stimulation, or both combined.[8,34,37,39]

The significantly different photoluminescence between Eu^{2+} and Eu^{3+} suggests that the reversible valence switching can be exploited for technical applications like radiation dosimetry and optical information storage by monitoring the variation of Eu^{2+}/Eu^{3+} emissions.[40,41] Indeed, Eu^{3+} shows sharp line emissions, mainly in the red region of the spectrum, while Eu^{2+} usually exhibits a tunable and broadband emission ranging from UV to NIR depending on the local

environment.[2] Therefore, understanding the influence of the illumination source on Eu, or another lanthanide featuring multiple valence states, is a fundamental issue.

Eu^{2+} or Ce^{3+} doped Cs_3CoCl_5-type phosphors have been widely studied in the past 20 years for the application in white LEDs due to their excitation band matching well with the NUV or blue emission of the chips, a high luminescence efficiency, and an especially tunable broadband emission owing to the flexible crystallographic environment of their cations.[42] Among them, $Sr_3SiO_5:Eu^{2+}$ has drawn extra attention since it was reported to exhibit persistent luminescence, OSL and so-called zero-thermal quenching behavior, all of which have been related to the electron transfer between Eu and trapping defects (or co-dopants).[43-45] In this work, the phenomena of photo-reduction ($Eu^{3+} \rightarrow Eu^{2+}$) and the following reverse process of photo- or thermally-induced oxidation ($Eu^{2+} \rightarrow Eu^{3+}$) are demonstrated in $Sr_3SiO_5:Eu^{3+}$. The influence of the illumination wavelength, the illumination duration and the annealing temperature on the Eu valence state is investigated in detail through photoluminescence and reflectance spectroscopy. Both the stability of the Eu^{2+} obtained by photo-reduction and the repeatability of alternating photo-reduction and oxidation are confirmed here. We also demonstrate the potential application for optical information storage based on these properties.

2. METHODS

PREPARATION

$Sr_3SiO_5:Eu^{3+}$ was synthesized by a high temperature solid state reaction, using high purity $SrCO_3$ (Alfa Aesar, 99.9%), SiO_2 (Alfa Aesar, 99.5%), and Eu_2O_3 (Alfa Aesar, 99.95 %) as precursors, and 3 mol% of BaF_2 was added as the flux.[46] In order to obtain $Sr_{2.99}Eu_{0.01}SiO_5$, stoichiometric mixtures of the precursors were weighed and ground, and subsequently ball-milled for 6 h with alcohol at a rotating speed of 300 rpm, followed by drying at 70 °C. After that, the obtained

powder was pre-calcined at 800 °C for 5 h and finally sintered at 1400 °C for 6 h in air. Then the sample was allowed to cool to room temperature naturally, and the final product was re-ground for further characterizations. Pressed pellets were also made from the final powder for specific optical measurements. $Sr_3SiO_5:Eu^{2+}$ and undoped Sr_3SiO_5 were prepared by the same procedure except for the use of a reducing atmosphere composed of 10% H_2 and 90% N_2 and the omission of precursor Eu_2O_3, respectively.

CHARACTERIZATIONS

The phase structure was determined by X-ray diffraction (XRD) using a Siemens D5000 diffractometer (40 kV, 40 mA) with Cu $K_{\alpha 1}$ radiation (λ = 0.154 nm). The microstructure was measured by using a Hitachi S-3400N scanning electron microscope (SEM), connected to a Thermo Scientific Noran 7 EDX analysis system. Photoluminescence (PL) emission and excitation (PLE) spectra of the pressed pellet were collected at room temperature using an Edinburgh Instrument FS920 spectrometer equipped with a monochromated 450 W Xe-arc lamp as the excitation source. All spectra were automatically corrected for detector response. The reflectance spectra of the pellet were measured at room temperature using a Perkin Elmer Lambda 1050 UV-vis-NIR spectrophotometer. Germicidal Hg lamp (254 nm emission line, 3 W) and 420 nm LED (full width at half maximum 20 nm, 5 V, 250 mA) were used for photo-reduction and oxidation, respectively. Ionizing radiation (X-ray) from a Siemens D5000 diffractometer (Cu anode, 40 kV and 40 mA) was used for photo-reduction as well. To investigate the wavelength-dependent photo-reduction/oxidation in $Sr_3SiO_5:Eu^{3+}$, we made an experimental setup schematically depicted in Figure 3a, having a wavelength tunable OPO laser (Ekspla NT340), shutters and a fiber based detection (QE65000 spectrometer, Ocean Optics) of the emission spectra under 420 nm LED excitation. As for the photo-oxidation experiments, the

pellet was pre-illuminated with 220 nm laser pulses for 10 min to ensure the formation of Eu^{2+} ions at the same level of saturation. Similarly, for the photo-reduction experiments, the pre-illumination was done with 420 nm laser pulses for 10 min to oxidize the Eu^{2+} ions formed during previous photo-reduction experiments. Then the pellet was illuminated with laser pulses of different wavelengths from the OPO (repetition rate of 1 Hz, pulse duration of 4 ns) for the photo-reduction/oxidation process. Two shutters were controlled by a LabVIEW program to alternately open and block the laser pulse and the probe light from a 420 nm LED. A pyroelectric energy sensor (ES220C, Thorlabs) was used to measure the energy of the laser pulse for each excitation wavelength. In combination with the number of pulses being recorded by LabVIEW, the wavelength dependent photo-reduction and oxidation experiments could be expressed in terms of the number of incident photons. Thermal oxidation experiments were performed by annealing the pre-illuminated (220 nm laser pulse for 10 min) pellet at different temperatures (50 to 600 °C) for 5 min in air. Photographs for the demonstration of optical information storage were taken with a Nikon D3200 camera in raw format. For illumination a 365 nm lamp (Hand-held UV lamp, Analytik Jena, 1.66 μW/mm^2) or daylight was used.

3. RESULTS AND DISCUSSION

Figure 1a provides the XRD patterns of $Sr_3SiO_5:Eu^{3+}$, un-doped Sr_3SiO_5 (both prepared in air) and $Sr_3SiO_5:Eu^{2+}$ (prepared under reducing atmosphere), which match well with the standard diffraction pattern of Sr_3SiO_5 (JCPDS 26-0984). The crystal structure of Sr_3SiO_5 (space group *P*4/*ncc*) is depicted in Figure 1b, which is composed of alternating layers of [Sr(2)O_6] octahedra

versus [Sr(1)O_6] octahedra and [SiO_4] tetrahedra along the *c*-axis.[42] The representative morphology of the obtained $Sr_3SiO_5:Eu^{3+}$ powder was examined by SEM (Figure 1c), and the corresponding EDX spectrum confirmed the presence and homogeneous distribution of Sr, Si and Eu.

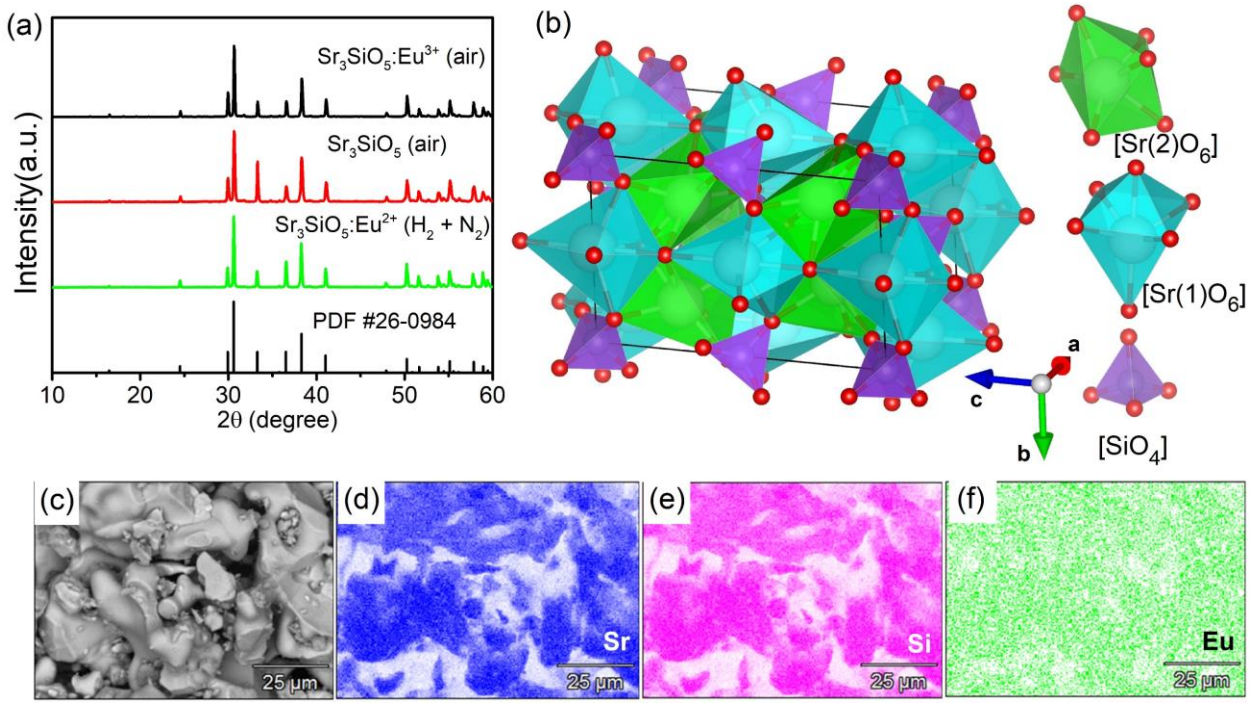

Figure 1. (a) XRD patterns of $Sr_3SiO_5:Eu^{3+}$, un-doped Sr_3SiO_5 and $Sr_3SiO_5:Eu^{2+}$, and reference pattern of Sr_3SiO_5 (JCPDS 26-0984). (b) Crystal structure of Sr_3SiO_5 and its building blocks [Sr(1)O_6], [Sr(2)O_6], [SiO_4] polyhedra drawn by VESTA software.[47] (c)-(f) SEM image and elemental mappings of $Sr_3SiO_5:Eu^{3+}$ powder by EDX.

The PL and PLE spectra for the $Sr_3SiO_5:Eu^{3+}$ prepared in air are given in Figure 2a. The emission spectrum consists of several line-emission peaks originating from $4f^6$-$4f^6$ transitions in Eu^{3+}. The relatively high intensity ratio of the Eu^{3+} emission transitions for $^5D_0 \rightarrow {}^7F_2$ compared to $^5D_0 \rightarrow {}^7F_1$ is consistent with the distortion of the [SrO_6] octahedra, given that Eu^{3+} ions are expected to occupy the Sr^{2+} sites.[42,48] For the excitation spectrum, the strong broad band centered

at 330 nm is ascribed to the Eu^{3+}-O^{2-} charge transfer state, while the weaker lines in the range from 375 to 470 nm correspond to the internal $4f^6$-$4f^6$ transitions of Eu^{3+}.[49] After illumination with a 254 nm lamp for 50 min, broad bands in the range of 380~550 nm (PLE spectrum) and 510~560 nm (PL spectrum) emerge when recording at the same excitation and emission wavelength as before (Figure 2a). The exact shapes of these new bands can be observed in Figure 2b by changing the excitation wavelength and monitoring wavelength. The emission band centered at 584 nm in Figure 2b can be attributed to a new type of luminescent center, and it exactly resembles the emission from the parity-allowed $4f^65d^1$-$4f^7$ transition of Eu^{2+} in Sr_3SiO_5 obtained by synthesizing under reducing atmosphere (Figure 2c). In addition, the PLE spectra for Eu^{2+} in these two cases also look similar. It should be mentioned that the PLE spectrum of 254 nm illuminated Sr_3SiO_5:Eu^{3+} was measured by monitoring the emission at 554 nm rather than at the emission peak wavelength of 584 nm to avoid the contribution from Eu^{3+}. From these results, we can thus unambiguously assign this emission band to newly formed Eu^{2+} by photo-reduction.[45]

The photo-reduction of Eu^{3+} also induces changes in the reflectance of the material. To quantify this, the reflectance of the material before and after illumination with 254 nm light was recorded and the spectra are shown in Figure 2d. To emphasize the differences in reflectance, the ratio of both spectra is also included. In addition to the absorption by the newly formed Eu^{2+}, also a stronger absorption centered around 380 nm can be observed. This band is also visible in the reflectance spectra of un-doped Sr_3SiO_5 and to a lesser extent in Sr_3SiO_5:Eu^{2+} (Figure 2e). The defect responsible for this absorption will be denoted as D^Q, and in the case of Sr_3SiO_5:Eu^{3+} (prepared under air), this defect likely traps an electron (forming D^{Q-1}) in order to balance the charge due to the substitution of Sr^{2+} by Eu^{3+}. Consequently, in Sr_3SiO_5:Eu^{3+} the characteristic

absorption of D^{Q} at 380 nm is missing (red curve in Figure 2d). Interestingly, once an electron is transferred to the Eu^{3+} under 254 nm illumination, the absorption band at 380 nm originating from D^{Q} shows up again (orange and green curves in Figure 2d), indicating that the following electron transfer process might be responsible for the observed valence changes:

$$D^{Q-1} + Eu^{3+} \rightarrow D^{Q} + Eu^{2+} \quad (1)$$

The dip in the Eu^{2+} PLE spectra around 380 nm might be a consequence of this defect absorption.

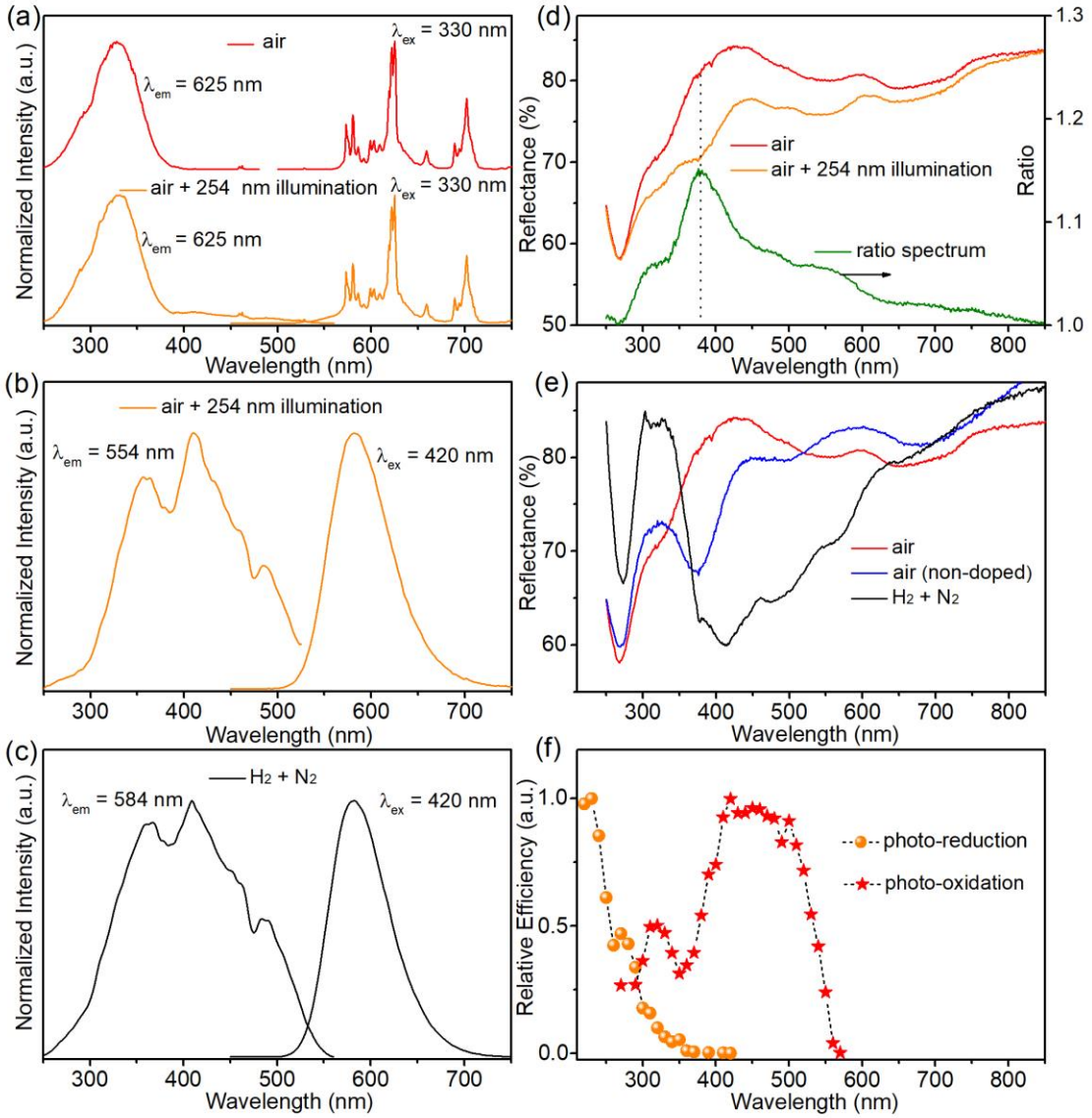

Figure 2. (a) Normalized PL and PLE spectra of $Sr_3SiO_5:Eu^{3+}$ (prepared in air) for Eu^{3+} emission before and after 254 nm illumination for 50 min. Normalized PL and PLE spectra of (b) 254 nm illuminated $Sr_3SiO_5:Eu^{3+}$ and (c) $Sr_3SiO_5:Eu^{2+}$ prepared in reducing atmosphere for Eu^{2+} emissions. (d) Reflectance spectra of $Sr_3SiO_5:Eu^{3+}$ before and after 254 nm light illumination and their ratio spectrum. (e) Reflectance spectra of non-doped Sr_3SiO_5 and $Sr_3SiO_5:Eu^{3+}$ prepared in

air, and $Sr_3SiO_5:Eu^{2+}$ prepared in reducing atmosphere. (f) Wavelength-dependent efficiency for photo-reduction/oxidation of $Sr_3SiO_5:Eu^{3+}$.

During the photo-reduction process described by Equation (1), the Eu^{3+} ions act as electron traps, and form metastable Eu^{2+} after trapping. The captured electron can also be detrapped ($Eu^{2+} \rightarrow Eu^{3+} + e^-$) with external optical and/or thermal stimulations. Wavelength-dependent photo-reduction/oxidation experiments may give us more underlying information about this process. Hence, a set-up with a tunable OPO pulsed laser was used (Figure 3a). The time dependent photo-reduction/oxidation under illumination is recorded by monitoring Eu^{2+} emission intensity. The results for photo-reduction/oxidation under illumination with 240 nm/460 nm laser pulse in this set-up are shown in Figure 3b and Figure 3c, respectively. Note that for these experiments, the sample was pre-illuminated by 420 nm or 220 nm laser pulses to minimize or maximize the Eu^{2+} luminescence prior to photo-reduction/oxidation, respectively.

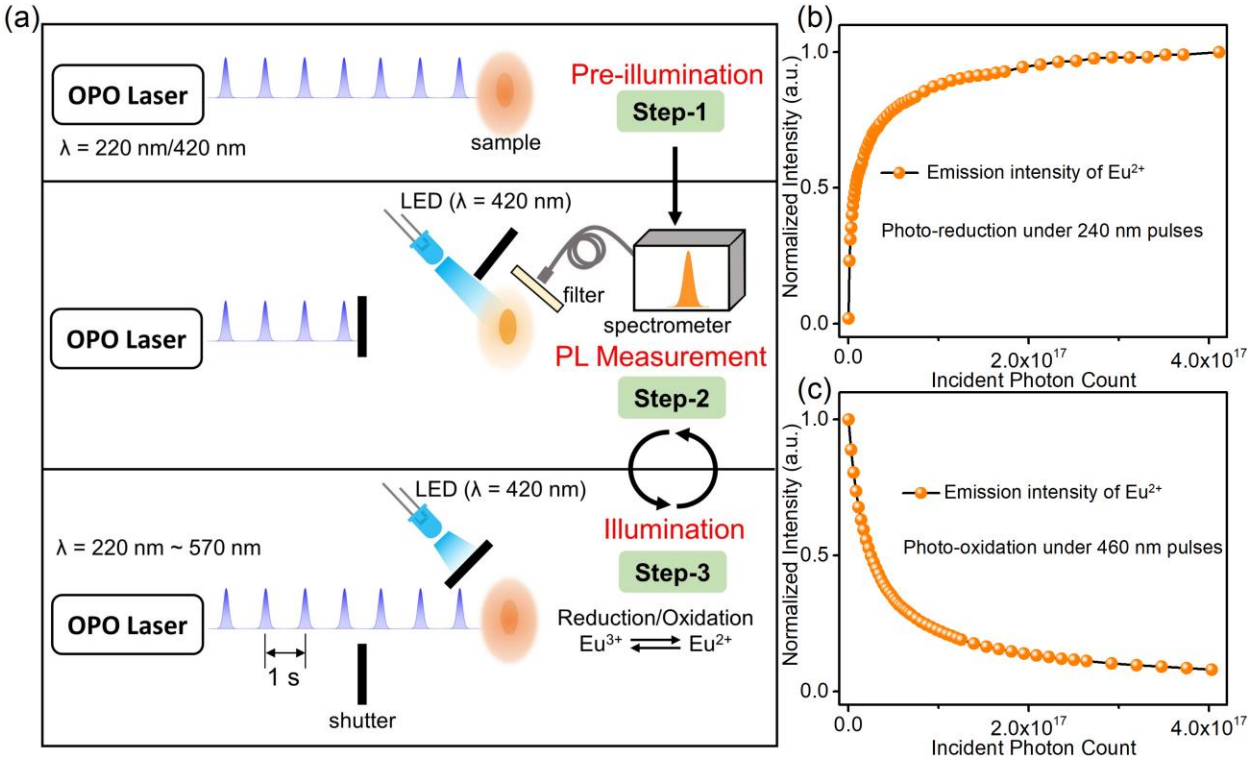

Figure 3. (a) Schematic diagram of the experimental setup for measurements of wavelength-dependent photo-reduction/oxidation in $Sr_3SiO_5:Eu^{3+}$. Eu^{2+} emission intensities as a function of incident photon counts of (b) 240 nm pulses for photo-reduction (pre-illuminated by 420 nm) and (c) 460 nm pulses for photo-oxidation (pre-illuminated by 220 nm)

The wavelength-dependent efficiency of the two processes was determined by comparing the Eu^{2+} luminescence intensity after exposure to a fixed amount of light, as presented in Figure 2f. A first observation is that the efficiency corresponding to photo-reduction decreases with increasing wavelength within the range of 220~350 nm. For longer wavelengths, the photo-reduction effect can hardly be observed. The creation of electron-hole pairs and the subsequent capture of an electron by Eu^{3+} cannot be responsible for such photo-reduction behavior since the energy of light used here (maximum 5.64 eV for 220 nm) is lower than the energy required for band-to-band transition in Sr_3SiO_5 (optical bandgap 5.98 eV).[49] There are then two possible explanations for the observed phenomena and they mostly differ in the assumed path that the transferred charge takes during the charge transfer process. The first possibility assumes the involvement of the Eu^{3+}-O^{2-} charge transfer (CT) state.[38] Excitation of this CT results in the formation of metastable Eu^{2+} and a hole being trapped by the defect D^{Q-1} (forming D^{Q}).[38] Similar explanations of the participation of the CT state have been proposed to interpret photo-reduction in $Y_2O_2S:Eu^{3+}$, $CaSO_4:Eu^{3+}$, Yb^{3+}-doped aluminosilicate optical fibers, and MeOH/EtOH solution with $Eu^{3+}/Yb^{3+}/Sm^{3+}$ and Cl^-.[25,36-38,50-53] In our case, however, the photo-reduction efficiency curve (Figure 2f) does not match the Eu^{3+}-O^{2-} CT excitation band (Figure 2a). Nevertheless, this possibility cannot be dismissed because the CT excitation band is unusually broad and it cannot be excluded that it consists of several contributions that might originate from inequivalent defects in the material.

Alternatively, a direct charge transfer between a Eu^{3+}-D^{Q-1} pair also belongs to the possibilities. Taking into account the characteristics of the photo-reduction spectrum, it is either possible that D^{Q-1} is excited, after which an electron is transferred to Eu^{3+} or that the charge transfer takes place after direct excitation into a Eu^{3+}- D^{Q-1} charge transfer level. This can explain why the photo-reduction spectrum does not overlap with the Eu^{3+}-O^{2-} charge transfer excitation band. Furthermore, if a charge transfer only takes place between Eu^{3+}-D^{Q-1} pairs that are in sufficiently close proximity to each other, this might also explain why only a small fraction of the Eu^{3+} can be reduced. In any case, it is clear that the oxidized defect D^{Q} strongly absorbs light at around 380 nm. Note that photo-reduction of a trivalent lanthanide following excitation of a defect that is subsequently oxidized, has already been verified convincingly in several lanthanide-codoped phosphors where the reduction of $Ln(1)^{3+}$ is initiated by excitation of the $Ln(2)^{2+}$, where the $Ln(2)^{2+}$ plays the same role as the unknown defect (D^{Q-1}) in our case, offering the electron for Eu^{3+}.[6,7,54]

The efficiency curve for wavelength-dependent photo-oxidation in Figure 2f shares common features with the PLE spectra for Eu^{2+} (Figure 2b,c), especially the strikingly similar threshold energy at around 2.18 eV (570 nm). It's safe to conclude that the photo-oxidation process is initiated by the excitation of Eu^{2+}. This is also consistent with the above-mentioned electron transfer process in lanthanides co-doped systems which occurs through excitation of divalent lanthanides ($Eu^{2+} + Ln^{3+} \rightarrow Eu^{3+} + Ln^{2+}$). However, the profile of this curve is not fully the same as the PLE spectra for Eu^{2+}. This might partly be due to the way the efficiency for the photo-oxidation was determined. In addition, for the wavelength range (270~350 nm) that shows both the photo-reduction and oxidation, the curve represents a dynamic equilibrium between the two competing photo-reduction and -oxidation processes, leading to the difference between this curve

and the PLE spectra for Eu^{2+} as well. The net effect of these two competing processes depends on the absorption abilities for the two different species that initiate the two opposite processes, which effectively limits the final concentration of Eu^{2+} that can be obtained by photo-reduction with a certain illumination wavelength. This is similar to what has been observed in persistent (or OSL) phosphors with the competition between trapping and detrapping, or photochromic materials with the competition between coloring and decoloring.[55-57] It is important to mention that in this region of overlap, the same equilibrium is obtained independent of whether the phosphor is initially in a maximally reduced or maximally oxidized state.

Not surprisingly there are also some similarities between the efficiency curve for photo-oxidation and the reflection spectrum of $Sr_3SiO_5:Eu^{2+}$ prepared in reducing atmosphere (black curve in Figure 2e) where the maximum absorption of $Sr_3SiO_5:Eu^{2+}$ is due to Eu^{2+}. As was already mentioned, this is not surprising as the following process is most likely responsible for the photo-oxidation: under illumination by 350~570 nm, Eu^{2+} is excited to the manifold of its excited $4f^65d^1$ states. Then it quickly relaxes and decays radiatively, or alternatively just transfers its electron to an unknown defect D^Q leaving the Eu^{2+} ion as Eu^{3+}.

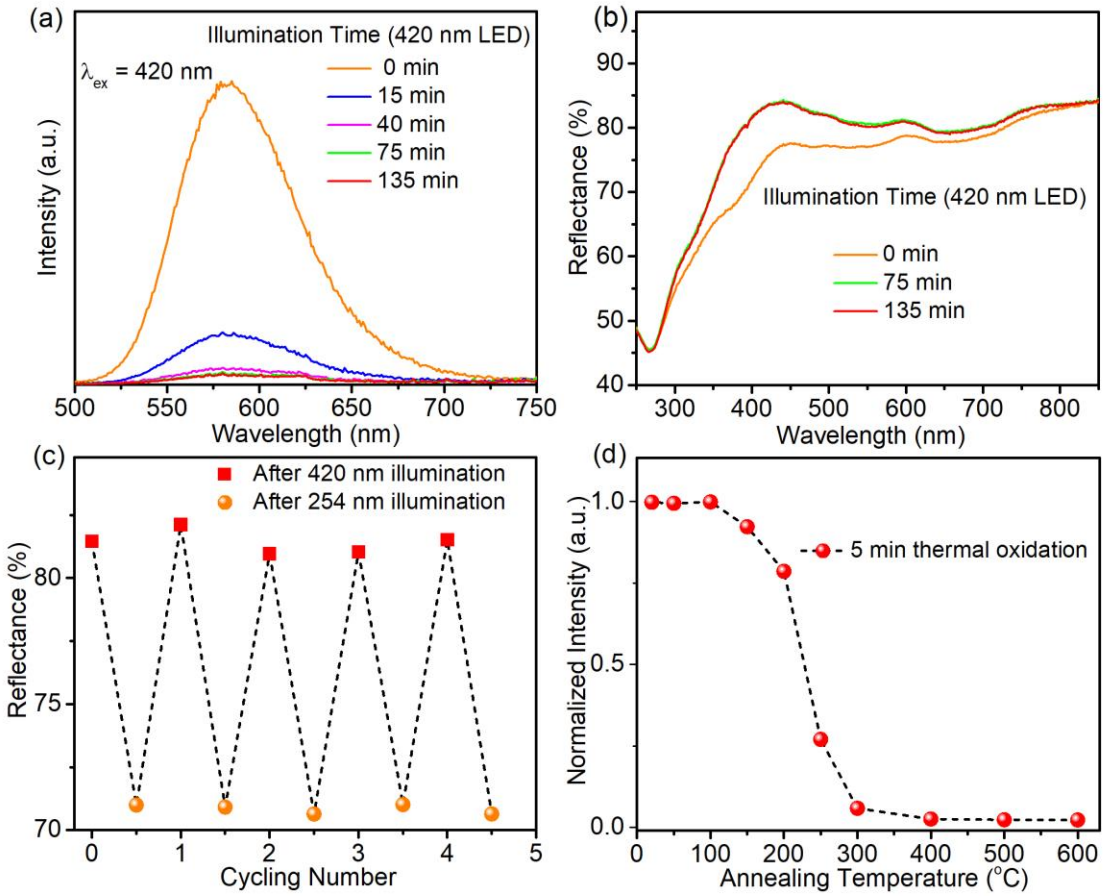

Figure 4. (a) PL spectra of 254 nm pre-illuminated (50 min) $Sr_3SiO_5:Eu^{3+}$ with different illumination time (420 nm LED) for photo-oxidation, and (b) the corresponding reflectance spectra. (c) Average reflectance values at 380~384 nm (where the strongest reflectance changes occur during illumination) for cycling test by alternating photo-reduction and photo-oxidation. (d) Dependence of the Eu^{2+} emission intensity (λ_{ex} = 420 nm) on annealing temperature in 220 nm pre-illuminated $Sr_3SiO_5:Eu^{3+}$.

The photo-oxidation (detrapping) in 254 nm pre-illuminated $Sr_3SiO_5:Eu^{3+}$ can also be achieved by illumination with a 420 nm LED. As is shown in Figure 4a, Eu^{2+} emission decreases substantially within the first 15 min, while illumination for longer than 75 min has only a limited

effect on further suppressing the remaining Eu^{2+} emission. This process is also illustrated by the variation of emission spectra (Figure S1) comprising a superposition of Eu^{2+} and Eu^{3+} emissions under 380 nm excitation, which was chosen in order to excite both the Eu^{2+} and the Eu^{3+} ions. The corresponding reflectance spectra are given in Figure 4b, further pointing out the negligible reflectance change with prolonged time after 75 min illumination. The difficulty to obtain complete photo-oxidation here is also observed in BaFCl:Sm^{3+} with pre-illumination for photo-reduction.[58] Similar phenomena are more common in OSL materials, and high temperature annealing may be required to address this issue.[59] For example, in OSL dosimeter phosphor MgB_4O_7:Ce^{3+},Li^+, optical bleaching is not able to empty all trapping centers which can affect the OSL sensitivity.[60,61] Consequently, residual signals due to incompletely bleached trapping centers appear in the following measurement. It is also interesting to check the stability of the photo-reduced Eu ions Sr_3SiO_5 over time. As is shown in Figure S2, both the reflectance spectra and PL intensity (λ_{ex} = 420 nm) of the 254 nm illuminated sample level off after 2 hours, and about 90 % of the initial emission from Eu^{2+} is still preserved, suggesting good stability of Eu^{2+} obtained by photo-reduction. The cycle of this reversible valence switching can be performed many times as indicated by the change of reflectance spectra in Figure S3. Figure 4c gives a closer look at the average reflectance value at 380~384 nm where the strongest change occurs during illumination. For the 420 nm illuminated state, the reflectance values at this region fluctuate within the range of 81.0 % to 82.1 %, while for the 254 nm illuminated state, the values are in the range from 70.6 % to 71.0 %. Therefore, good repeatability for alternating illumination with 254 nm UV light and 420 nm violet light is also guaranteed.

As stated previously, besides photo-oxidation, thermal stimulation also allows to effectively re-oxidize the Ln^{2+} obtained by photo-reduction back to Ln^{3+}, as in the reported case of

$LuPO_4:Eu^{3+}$ or $Sr_2SiO_4:Eu^{3+}$.[34,37] To find out the thermal effect on the illuminated $Sr_3SiO_5:Eu^{3+}$, the 220 nm pre-illuminated sample was annealed at different temperatures in air for 5 min, followed by measuring the emission spectra at room temperature. It was observed that the intensity of Eu^{2+} orange–yellow emission starts to decrease after annealing at around 150 °C (Figure 4d), and complete thermal oxidation of Eu^{2+} occurs at around 400 °C, indicating that the thermal stability of the trapped charges is much larger than that encountered in a typical persistent phosphor such as $SrAl_2O_4:Eu^{2+},Dy^{3+}$, where a considerable detrapping is already found at room temperature.[7] This observation is also in line with the good stability of the 254 nm illuminated sample at room temperature as mentioned before (Figure S2).

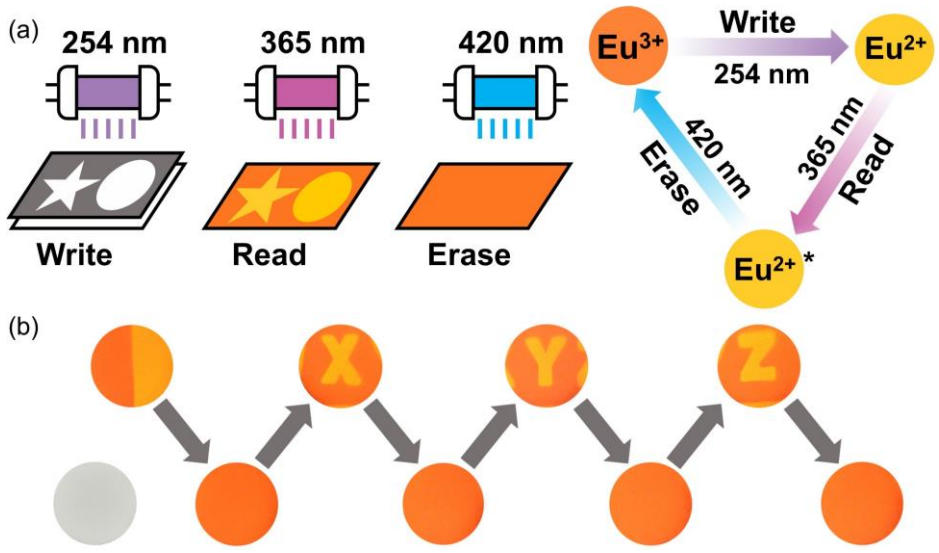

Figure 5. (a) Schematic diagram for the application of optical information storage. (b) Photographs of a pellet under 365 nm lamp illumination with/without latent images. Photograph of the same pellet without any additional illumination under daylight is also given here.

Given the stability of Eu^{2+} obtained by photo-reduction, the repeatability of Eu^{2+}/Eu^{3+} valence switching and different emission of Eu^{2+}/Eu^{3+} as we have shown above, $Sr_3SiO_5:Eu^{3+}$ can be a

good candidate for the application of optical information storage. The schematic diagram for this application is shown in Figure 5a. During the "write" process, the phosphor is illuminated by a 254 nm lamp with a photomask for several minutes. The photo-reduction of $Eu^{3+} \rightarrow Eu^{2+}$ only occurs in the area that has been illuminated. Then based on different distribution and emission color of Eu^{2+} and Eu^{3+}, the latent image can be well visualized when illuminated with 365 nm ("read" process). More importantly, the information can be readily erased by 420 nm light, thus the materials can be reused again. Figure 5b demonstrates the photographs (under 365 nm lamp illumination) of the same pellet with different latent images and subsequent removal of the information, and the 254 nm-illuminated area was demonstrated with orange–yellow emission color. It is worth noting that the emission ratio of Eu^{2+}/Eu^{3+} instead of the absolute emission intensity of Eu^{2+} can be used to determine the area that has been illuminated by 254 nm light, therefore this material may serve as the medium for self-calibrated optical information storage or for UV-C dosimetry. In addition, X-ray-induced photo-reduction of Eu^{3+} was also observed (Figure S4), indicating its potential application in X-ray imaging or X-ray dosimetry.[34]

Actually, the conversion ratio of Eu^{3+} to Eu^{2+} is not high under 254 nm lamp illumination, otherwise the excitation spectrum (Fig. 2a, λ_{em} = 625 nm) after illumination would be dominated by Eu^{2+}. The conversion ratio may be on the same order of magnitude as the ratio of Eu^{2+} to Eu^{3+} in the typical persistent phosphor $SrAl_2O_4:Eu^{2+},Dy^{3+}$ during charging.[62] However, from the point of application, the problem of a low conversion ratio can be circumvented by choosing the excitation wavelengths that favor Eu^{2+} emission rather than Eu^{3+} emission. Moreover, the high absorption cross section and emission efficiency of Eu^{2+} result in an intense emission when compared to Eu^{3+}. It should be mentioned that the results of wavelength-dependent photo-reduction/oxidation in Figure 2f give us good guidance to selectively choose the appropriate

wavelengths for the write, read and erase steps in the optical information storage process. Especially for the reading step, even though photo-oxidation of Eu^{2+} occurs to some extent during reading, this effect can be alleviated by using light in the spectral range where photo-oxidation is less efficient, thus the optical information can be kept even after reading multiple times.

4. CONCLUSION

Reversible valence switching between Eu^{2+} and Eu^{3+} in $Sr_3SiO_5:Eu^{3+}$ prepared in air was achieved here by optical and thermal stimulations. The photo-reduction of Eu^{3+} is observed under illumination of 220~350 nm light, and shorter wavelengths result in more efficient electron transfer from non-oxidized defects D^{Q-1} to Eu^{3+}. Simultaneously with the photo-reduction an absorption band appears at around 380 nm which is tentatively ascribed to the oxidized electron donor D^{Q}. Photo-oxidation occurs within the whole range of the Eu^{2+} excitation/absorption spectrum (270~570 nm), and thus the process can be safely ascribed to the excitation of Eu^{2+}, followed by an electron transfer from Eu^{2+} to the oxidized defect D^{Q}. The wavelength-dependent competition between photo-reduction and photo-oxidation limits the number of Eu^{3+} ions that can be photo-reduced, which is evidenced by the by the spectral region where both effects occur simultaneously (270~350 nm). Reflectance spectra at different fading times and annealing temperature-dependent photoluminescence measurements show good stability for the Eu^{2+} ions obtained by photo-reduction. Cycle measurements for valence switching confirm the repeatability of this photo-oxidation and reduction behavior. The application of these phosphors for optical information storage based on these above-mentioned good performances was demonstrated. This work provides new insights into the valence change process of Eu^{2+}/Eu^{3+} in

the $Sr_3SiO_5:Eu^{3+}$ phosphor, and a transferable experimental approach to disentangle the wavelength dependency of photo-oxidation and photo-reduction for other lanthanide-activated luminescent materials has been demonstrated. However, a dedicated study of the effect of the dopant concentration on the amount of Eu that can be photo-reduced is still required.

TOC Graphic

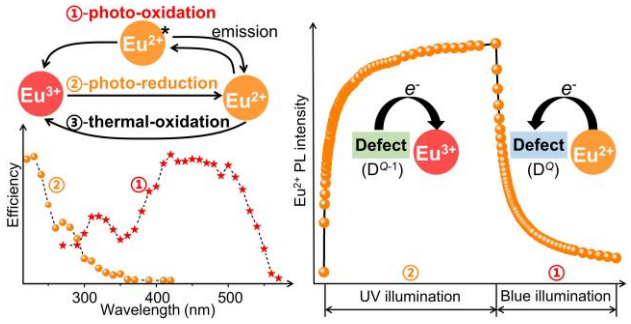

ASSOCIATED CONTENT

Supporting Information.

PL spectra (Figure S1) and fading effect (Figure S2) of 254 nm pre-illuminated $Sr_3SiO_5:Eu^{3+}$; Reflectance spectra for cycling test (Figure S3); PL spectra before and after X-ray irradiation (PDF).

AUTHOR INFORMATION

Corresponding Author

Philippe Smet

Email: Philippe.Smet@ugent.be

Notes

The authors declare no competing financial interest.

ACKNOWLEDGMENT

The authors acknowledge the financial support from the China Scholarship Council (Grant No. 201706150080) and the FWO (Fund for Scientific Research–Flanders, Hercules project I002418N and research project G0F9322N).

REFERENCES

(1) Blasse, G.; Grabmaier, B. C. *Luminescent Materials*; SpringerVerlag: Berlin, 1994.

(2) Yen, W. M.; Shionoya, S.; Yamamoto, H. *Phosphor handbook*; CRC Press: Boca Raton, FL, 2006.

(3) Cotton, S. *Lanthanide and Actinide Chemistry*; John Wiley & Sons, Ltd.: Chichester, England, 2006.

(4) Morss, L. R. Thermochemical Properties of Yttrium, Lanthanum, and the Lanthanide Elements and Ions. *Chem. Rev.* **1976**, *76*, 827−841.

(5) Suta, M.; Wickleder, C. Synthesis, Spectroscopic Properties and Applications of Divalent Lanthanides Apart from Eu^{2+}. *J. Lumin.* **2019**, *210*, 210−238.

(6) Joos, J. J.; Korthout, K.; Amidani, L.; Glatzel, P.; Poelman, D.; Smet, P. F. Identification of Dy^{3+}/Dy^{2+} as Electron Trap in Persistent Phosphors. *Phys. Rev. Lett*. **2020**, *125*, 033001.

(7) Van der Heggen, D.; Zilenaite, R.; Ezerskyte, E.; Fritz, V.; Korthout, K.; Vandenberghe, D.; De Grave, J.; Garrevoet, J.; Vincze, L.; Poelman, D.; et al. A Standalone, Battery-Free Light Dosimeter for Ultraviolet to Infrared Light. *Adv. Funct. Mater.* **2022**, *32*, 2109635.

(8) Winnacker, A.; Shelby, R. M.; Macfarlane, R. M. Photon-Gated Hole Burning: a New Mechanism Using Two-Step Photoionization. *Opt. Lett.* **1985**, *10*, 350−352.

(9) Welber, B. Reversible Phototransfer of Electrons between Rare Earth Ions in CaF_2. *J. Chem. Phys.* **1965**, *42*, 4262−4264.

(10) Poolton, N. R. J.; Bos, A. J. J.; Jones, G. O.; Dorenbos, P. Probing Electron Transfer Processes in YPO_4:Ce, Sm by Combined Synchrotron – Laser Excitation Spectroscopy. *J. Phys. Condens. Matter* **2010**, *22*, 185403.

(11) Yuan, L.; Jin, Y.; Su, Y.; Wu, H.; Hu, Y.; Yang, S. Optically Stimulated Luminescence Phosphors: Principles, Applications, and Prospects. *Laser Photonics Rev.* **2020**, *14*, 2000123.

(12) Yu, D. C.; Rabouw, F. T.; Boon, W. Q.; Kieboom, T.; Ye, S.; Zhang, Q. Y.; Meijerink, A. Insights into The Energy Transfer Mechanism in Ce^{3+}-Yb^{3+} Codoped YAG Phosphors. Phys. Rev. B: Condens. *Matter Mater. Phys.* **2014**, *90*, 165126.

(13) Barandiarán, Z.; Seijo, L. Intervalence Charge Transfer Luminescence: Intervalence Charge Transfer Luminescence: Interplay Between Anomalous and 5*d*−4*f* Emissions in Yb-Doped Fluorite-Type Crystals. *J. Chem. Phys.* **2014**, *141*, 234704.

(14) Joos, J. J.; Van der Heggen, D.; Martin, L. I. D. J.; Amidani, L.; Smet, P. F.; Barandiarán, Z.; Seijo, L. Broadband Infrared LEDs Based on Europium-to-Terbium Charge Transfer Luminescence. *Nat. Commun.* **2020**, *11*, 3647.

(15) Blasse, G. Energy Transfer from Ce^{3+} to Eu^{3+} in (Y, Gd)F_3. *Phys. Status Solidi A* **1983**, *75*, K41−K43.

(16) Vergeer, P.; Babin, V.; Meijerink, A. Quenching of Pr^{3+} $^1S_0$ Emission by Eu^{3+} and Yb^{3+}. *J. Lumin.* **2005**, *114*, 267–274.

(17) Joos, J. J.; Seijo, L.; Barandiarán, Z. Direct Evidence of Intervalence Charge-Transfer States of Eu-Doped Luminescent Materials. *J. Phys. Chem. Lett.* **2019**, *10*, 1581–1586.

(18) Joos, J. J.; Neefjes, I.; Seijo, L.; Barandiarán, Z. Charge Transfer from Eu^{2+} to Trivalent Lanthanide Co-Dopants: Systematic Behavior across the Series. *J. Chem. Phys.* **2021**, *154*, 064704.

(19) Li, S. X.; Wang, L.; Tang, D. M.; Cho, Y. J.; Liu, X. J.; Zhou, X. T.; Lu, L.; Zhang, L.; Takeda, T.; Hirosaki, N.; et al. Achieving High Quantum Efficiency Narrow-Band *β*-Sialon:

Eu^{2+} Phosphors for High-Brightness LCD Backlights by Reducing the Eu^{3+} Luminescence Killer. *Chem. Mater.* **2018**, *30*, 494−505.

(20) Yamashita, N. Coexistence of the Eu^{2+} and Eu^{3+} Centers in the CaO:Eu Powder Phosphor. *J. Electrochem. Soc.* **1993**, *140*, 840–843.

(21) Amidani, L.; Korthout, K.; Joos, J. J.; Linden, M. V. D.; Sijbom, H. F.; Meijerink, A.; Poelman, D.; Smet, P. F.; Glatzel, P. Oxidation and Luminescence Quenching of Europium in $BaMgAl_{10}O_{17}$ Blue Phosphors. *Chem. Mater.* **2017**, *29*, 10122−10129.

(22) Avci, N.; Korthout, K.; Newton, M. A.; Smet, P. F.; Poelman, D. Valence States of Europium in $CaAl_2O_4$:Eu Phosphors. *Opt. Mater. Express* **2012**, *2*, 321−330.

(23) van de Haar, M. A.; Tachikirt, M.; Berends, A. C.; Krames, M. R.; Meijerink, A.; Rabouw, F. T. Saturation Mechanisms in Common LED Phosphors. *ACS Photonics* **2021**, *8*, 1784–1793.

(24) Engholm, M.; Norin, L.; Åberg, D. Strong UV Absorption and Visible Luminescence in Ytterbium-Doped Aluminosilicate Glass Under UV Excitation. *Opt. Lett.* **2007**, *32*, 3352−3354.

(25) Rybaltovsky, A. A.; Bobkov, K. K.; Velmiskin, V. V.; Umnikov, A. A.; Shestakova, I. A.; Guryanov, A. N.; Likhachev, M. E.; Bubnov, M. M.; Dianov, E. M. The Yb-Doped Aluminosilicate Fibers Photodarkening Mechanism Based on the Charge-Transfer State Excitation. *Proc. SPIE*, **2014**, *8961*, 896116.

(26) Zavala, L. A.; Fernandez, P.; Novitskaya, E.; Díaz, J. N.; Herrera, M.; Graeve, O. A. Interconfigurational and Intraconfigurational Transitions of Yb^{2+} and Yb^{3+} Ions in Hydroxyapatite: A Cathodoluminescence Study. *Acta Mater.* **2017**, *135*, 35−43.

(27) Kaur Behrh, G.; Serier-Brault, H.; Jobic, S.; Gautier, R. A Chemical Route Towards Single-Phase Materials with Controllable Photoluminescence. *Angew. Chem., Int. Ed.* **2015**, *127*, 11663−11665.

(28) Pei, Z. W.; Zeng, Q. H.; Su, Q. The Application and a Substitution Defect Model for $Eu^{3+} \rightarrow Eu^{2+}$ Reduction in Non-Reducing Atmospheres in Borates Containing BO_4 Anion Groups. *J. Phys. Chem.* Solids **2000**, *61*, 9−12.

(29) Suta, M.; Lavoie-Cardinal, F.; Wickleder, C. Underestimated Color Centers: Defects as Useful Reducing Agents in Lanthanide-Activated Luminescent Materials. *Angew. Chem., Int. Ed.* **2020**, *59*, 10949−10954.

(30) Zhang, Y.; Li, X.; Li, K.; Lian, H.; Shang, M.; Lin, J. Crystal-Site Engineering Control for the Reduction of Eu^{3+} to Eu^{2+} in $CaYAlO_4$: Structure Refinement and Tunable Emission Properties. *ACS Appl. Mater. Interfaces* **2015**, *7*, 2715−2725

(31) Zhao, M.; Xia, Z.; Huang, X.; Ning, L.; Gautier, R.; Molokeev, M. S.; Zhou, Y.; Chuang, Y.-C.; Zhang, Q.; Liu, Q.; et al. Li Substituent Tuning of LED Phosphors with Enhanced Efficiency, Tunable Photoluminescence, and Improved Thermal Stability. *Sci. Adv.* **2019**, *5*, eaav0363.

(32) Smet, P. F.; Avci, N.; Van den Eeckhout, K.; Poelman, D. Extending the Afterglow in $CaAl_2O_4$:Eu, Nd Persistent Phosphors by Electron Beam Annealing. *Opt. Mater. Express* **2012**, *2*, 1306−1313.

(33) Jia, H.; Chen, Z.; Liu, Z. L.; Zhao, J. G.; Ding, C. L.; Yang, H. F.; Zhang, W. Y.; Liu, X. F.; Qiu, J. R. CaF_2:Eu Films Shine Novel Blue, White or Red Luminescence Though Adjustment of the Valence State of Eu Ions Using the Electro-Deposition Method. *J. Mater. Chem. C* **2017**, *5*, 12085−12089.

(34) Laguta, V.; Buryi, M.; Nikl, M.; Zeler, J.; Zych, E.; Bettinelli, M. Electron and Hole Trapping in Eu- or Eu,Hf-Doped $LuPO_4$ and YPO_4 Tracked by EPR and TSL Spectroscopy. *J. Mater. Chem. C* **2019**, *7*, 11473–11482.

(35) Qiu, J. R.; Kojima, K.; Miura, K.; Mitsuyu, T.; Hirao, K. Infrared Femtosecond Laser Pulse-Induced Permanent Reduction of Eu^{3+} to Eu^{2+} in a Fluorozirconate Glass. *Opt. Lett.* **1999**, *24*, 786−788.

(36) Nakashima, N.; Yamanaka, K.; Yatsuhashi, T. Reduction of Yb(III) to Yb(II) by Two-Color Two-Photon Excitation. *J. Phys. Chem. A* **2013**, *117*, 8352–8359.

(37) Nag, A.; Kutty, T. R. N. The Light Induced Valence Change of Europium in Sr_2SiO_4:Eu Involving Transient Crystal Structure. *J. Mater. Chem.* **2004**, *14*, 1598−1604.

(38) Struck, C. W.; Fonger, W. H. Dissociation of Eu^{+3} Charge-Transfer State in Y_2O_2S and La_2O_2S into Eu^{+2} and a Free Hole. *Phys. Rev. B: Condens. Matter Mater. Phys.* **1971**, *4*, 22.

(39) Schuyt, J. J.; Williams, G. V. M. Quenching of the Sm^{2+} Luminescence in $NaMgF_3$:Sm via Photothermal Ionization: Alternative Method to Determine Divalent Lanthanide Trap Depths. *Appl. Phys. Lett.* **2019**, *115*, 181104.

(40) Chen, W. Optical Storage Based on Reversible Optical Processes in Eu^{3+} Doped Nanoparticles. *Rev. Nanosci. Nanotechnol.* **2013**, *2*, 143−146.

(41) Ingle, N. B.; Omanwar, S. K.; Muthal, P. L.; Dhopte, S. M.; Kondawar, V. K.; Gundurao, T. K.; Moharil, S. V. Synthesis of $CaSO_4$:Dy, $CaSO_4$:Eu^{3+} and $CaSO_4$:Eu^{2+} Phosphors. *Radiat. Meas.* **2008**, *43*, 1191–1197.

(42) Viswanath, N. S. M.; In, J. H.; Kim, H. J.; Grandhi, G. K.; Im, W. B. Critical Review—A Promising Cs_3CoCl_5 Prototype Phosphor toward the Discovery of Next-Generation LED Phosphor. *ECS J. Solid State Sci. Technol.* **2020**, *9*, 016016.

(43) Sun, X.; Zhang, J.; Zhang, X.; Luo, Y.; Wang, X. Long Lasting Yellow Phosphorescence and Photostimulated Luminescence in $Sr_3SiO_5:Eu^{2+}$ and $Sr_3SiO_5:Eu^{2+}$, Dy^{3+} Phosphors. *J. Phys. D: Appl. Phys.* **2008**, *41*, 195414.

(44) Wang, Z.; Song, Z.; Ning, L.; Liu, Q. Sunlight-Activated Yellow Long Persistent Luminescence from Nb-Doped $Sr_3SiO_5:Eu^{2+}$ for Warm-Color Mark Applications. *J. Mater. Chem. C* **2020**, *8*, 1143−1150.

(45) Fan, X. T.; Chen, W. B.; Xin, S. Y.; Liu, Z. C.; Zhou, M.; Yu, X. D.; Zhou, C.; Xu, X. H.; Qiu, J. B. Achieving Long-Term Zero-Thermal Quenching with the Assistance of Carriers from Deep Traps. *J. Mater. Chem. C* **2018**, *6*, 2978−2982.

(46) Kim, H.-H.; Chung, K.-S.; Lee, S.-W.; Kim, B.-G. Influence of Fluxing Agents in $Sr_3SiO_5:Eu^{2+}$ Phosphors for Fabrication of Warm White Light Emitting Diodes. *J. Korean Ceram. Soc.* **2012**, *49*, 105–110.

(47) Momma, K.; Izumi, F. VESTA 3 for Three-Dimensional Visualization of Crystal, Volumetric and Morphology Data. *J. Appl. Crystallogr.* **2011**, *44*, 1272−1276.

(48) Tanner, P. A. Some Misconceptions Concerning the Electronic Spectra of Tri-Positive Europium and Cerium. *Chem. Soc. Rev.* **2013**, *42*, 5090−5101.

(49) Luo, H.; Bos, A. J. J.; Dobrowolska, A.; Dorenbos, P. Low Temperature VUV Photoluminescence and Thermoluminescence of UV Excited Afterglow Phosphor $Sr_3Al_xSi_{1-x}O_5:Ce^{3+},Ln^{3+}$ (Ln = Er, Nd, Sm, Dy and Tm). *Phys. Chem. Chem. Phys.* **2015**, *17*, 15419−15427.

(50) Nakashima, N.; Nakamura, S.; Sakabe, S.; Schillinger, H.; Hamanaka, Y.; Yamanaka, C.; Kusaba, M.; Ishihara, N.; Izawa, Y. Multiphoton Reduction of Eu^{3+} to Eu^{2+} in Methanol

Using Intense, Short Pulses from a Ti:Sapphire Laser. *J. Phys. Chem. A* **1999**, *103*, 3910–3916.

(51) Nishida, D.; Yamade, E.; Kusaba, M.; Yatsuhashi, T.; Nakashima, N. Reduction of Sm^{3+} to Sm^{2+} by an Intense Femtosecond Laser Pulse in Solution. *J. Phys. Chem. A* **2010**, *114*, 5648−5654.

(52) Tsuta, M.; Nakamura, S.; Kato, A. Micronization of $KSrPO_4$:Eu and $KBaPO_4$:Eu Phosphor Particles for White Light-Emitting Diodes by Pulsed Laser Ablation in Liquid. *Opt. Laser Technol.* **2021**, *135*, 106725.

(53) Danby, R. J. Ultraviolet-Induced Charge Transfer in $CaSO_4$:Eu. *J. Phys. C: Solid State Phys*. **1988**, *21*, 485.

(54) Joos, J. J.; Van der Heggen, D.; Amidani, L.; Seijo, L.; Barandiarán, Z. Elucidation of the Electron Transfer Mechanism in Eu^{2+} and Sm^{3+} Codoped CaF_2: A Step Towards Better Understanding of Trapping and Detrapping in Luminescent Materials. *Phys. Rev. B: Condens. Matter Mater. Phys.* **2021**, *104*, L201108.

(55) Van der Heggen, D.; Joos, J. J.; Smet, P. F. Importance of Evaluating the Intensity Dependency of the Quantum Efficiency: Impact on LEDs and Persistent Phosphors. *ACS Photonics* **2018**, *5*, 4529−4537.

(56) Tydtgat, C.; Meert, K. W.; Poelman, D.; Smet, P. F. Optically Stimulated Detrapping during Charging of Persistent Phosphors. *Opt. Mater. Express* **2016**, *6*, 844.

(57) Yang, Z.; Hu, J.; Martin, L. I. D. J.; Van der Heggen, D.; Poelman, D. Realizing Nondestructive Luminescence Readout in Photochromic Ceramics via Deep Ultraviolet Excitation for Optical Information Storage. *J. Mater. Chem. C* **2021**, *9*, 14012–14020.

(58) Riesen, H.; Badek, K.; Monro, T. M.; Riesen, N. Highly Efficient Valence State Switching of Samarium in BaFCl:Sm Nanocrystals in the Deep UV for Multilevel Optical Data Storage. *Opt. Mater. Express* **2016**, *6*, 3097.

(59) Akselrod, M. S. Fundamentals of Materials, Techniques, and Instrumentation for OSL and FNTD Dosimetry. *AIP Conf. Proc.* **2011**, *1345*, 274-302.

(60) Shrestha, N.; Vandenbroucke, D.; Leblans, P.; Yukihara, E. G. Feasibility Studies on the Use of MgB_4O_7:Ce,Li-Based Films in 2D Optically Stimulated Luminescence Dosimetry. *Phys. Open* **2020**, *5*, 100037.

(61) Gustafson, T. D.; Milliken, E. D.; Jacobsohn, L. G.; Yukihara, E. G. Progress and Challenges towards the Development of a New Optically Stimulated Luminescence (OSL) Material Based on MgB_4O_7:Ce,Li. *J. Lumin.* **2019**, *212*, 242–249.

(62) Van der Heggen, D.; Joos, J. J.; Rodríguez Burbano, D.; Capobianco, J.; Smet, P. F. Counting the Photons: Determining the Absolute Storage Capacity of Persistent Phosphors. *Materials* **2017**, *10*, 867.